
From Pixels to Torques: Policy Learning with Deep Dynamical Models

Niklas Wahlström

Division of Automatic Control, Linköping University, Linköping, Sweden

NIKWA@ISY.LIU.SE

Thomas B. Schön

Department of Information Technology, Uppsala University, Sweden

THOMAS.SCHON@IT.UU.SE

Marc Peter Deisenroth

Department of Computing, Imperial College London, United Kingdom

M.DEISENROTH@IMPERIAL.AC.UK

Abstract

Data-efficient learning in continuous state-action spaces using very high-dimensional observations remains a key challenge in developing fully autonomous systems. In this paper, we consider one instance of this challenge, the pixels-to-torques problem, where an agent must learn a closed-loop control policy from pixel information only. We introduce a data-efficient, model-based reinforcement learning algorithm that learns such a closed-loop policy directly from pixel information. The key ingredient is a deep dynamical model that uses deep auto-encoders to learn a low-dimensional embedding of images jointly with a prediction model in this low-dimensional feature space. This joint learning ensures that not only static properties of the data are accounted for, but also dynamic properties. This is crucial for long-term predictions, which lie at the core of the adaptive model predictive control strategy that we use for closed-loop control. Compared to state-of-the-art reinforcement learning methods, our approach learns quickly, scales to high-dimensional state spaces and facilitates fully autonomous learning from pixels to torques.

ages) to summarize knowledge about the surrounding environment and the system’s behavior in this environment, (2) make decisions based on uncertain and incomplete information, (3) take new information into account for learning and adaptation. Effectively, any fully autonomous system has to close this perception-action-learning loop without relying on specific human expert knowledge. The *pixels to torques problem* identifies key aspects of an autonomous system: autonomous thinking and decision making using sensor measurements only, intelligent exploration and learning from mistakes. More specifically, Brock (2011) defines the pixels-to-torques problem as follows:

“The expression ‘pixels to torques’ might be the simplest way of describing the high-level agenda of research at the intersection of AI and robotics: How can we create an agent capable of taking all of its sensor input and turning it into meaningful and purposeful motion to affect the world and perform active sensing? How can such an agent explore the world, learn from its mistakes, or apply past experiences to novel situations?”

To date, there is no fully autonomous system that convincingly closes the perception-action-learning loop and solves the pixels-to-torques problem in continuous state-action spaces, which are the natural domains in robotics.

A promising approach toward solving the pixels to torques problem is Reinforcement Learning (RL) (Sutton & Barto, 1998), a principled mathematical framework that deals with fully autonomous learning from trial and error. However, one practical shortcoming of many existing RL algorithms is that they require a lot of trials to learn good policies, which is prohibitive when working with real-world mechanical plants or robots.

First promising results in the context of fully autonomous learning are already available, especially in the context

1. Introduction

The vision of fully autonomous and intelligent systems that learn by themselves has influenced AI and robotics research for many decades. To devise fully autonomous systems, it is necessary to (1) process perceptual data (e.g., im-

of computer games, where human-level game strategies are learned autonomously, purely based on pixel information (Mnih et al., 2013). Moreover, Lange & Riedmiller (2010) presented an approach, which learns good discrete actions to control a slot car based on raw images, employing deep architectures for finding compact low-dimensional representations. However, these approaches are fairly data inefficient, either requiring data collection from millions of experiments or relying on discretization and very low-dimensional feature spaces, which limits their applicability to mechanical systems.

To learn control policies from pixel information only while keeping the number of experiments small, we need to use the available data efficiently. One way of doing this is to learn forward models of the underlying dynamical system, which is then used for internal simulations. These ideas have been successfully applied to RL problems in control and robotics by Atkeson & Schaal (1997), Bagnell & Schneider (2001), Deisenroth & Rasmussen (2011) and Pan & Theodorou (2014), for instance. All these methods use heuristic or engineered low-dimensional features, but they do not easily scale to data-efficient RL using pixel information only since even “small” images possess thousands of dimensions.

A common way of dealing with high-dimensional data is to learn low-dimensional feature representations. Deep learning architectures, such as deep neural networks (Hinton & Salakhutdinov, 2006), stacked auto-encoders (Bengio et al., 2007; Vincent et al., 2008), or convolutional neural networks (LeCun et al., 1998), are the current state of the art in learning parsimonious representations of high-dimensional data. Deep learning has been successfully applied to image, text and speech data in commercial products, e.g., by Google, Amazon and Facebook.

In this paper, we consider the setting where we have access to video data from a robotic agent moving about. The objective is to learn a closed-loop control policy from pixel information only, such that the agent solves a particular task, while keeping the number of trials low. To solve this task data efficiently, we propose to learn compact representations of images, which we use to learn predictive models and controllers in this lower-dimensional feature space. In particular, our approach to learning from pixels to torques is to jointly learn a lower-dimensional embedding of images and a transition function that we can use for internal simulation of the dynamical system. For this purpose, we employ deep auto-encoders for the lower-dimensional embedding and a multi-layer feed-forward neural network for the transition function. We use this deep dynamical model as a generative model for trajectories and apply an adaptive model-predictive-control (MPC) algorithm for online closed-loop control of the robotic agent, which is practi-

cally based on pixel information only.

2. Problem Set-up and Objective

We consider a classical N -step finite-horizon RL setting, where an agent attempts to solve a particular task by trial and error. In particular, our objective is to find a (closed-loop) policy π^* that minimizes the long-term cost

$$V^\pi = \sum_{t=0}^{N-1} f_0(x_t, u_t)$$

where f_0 denotes an immediate cost, x_t denotes the continuous-valued state of the system, and u_t represents the continuous control inputs.

The learning agent faces the following additional challenges: (a) the agent does not have access to the true state, but perceives the environment only through high-dimensional pixel information (images), (b) a good control policy is required in only a few trials. This setting is practically relevant, e.g., when the agent is a robot that is monitored by a video camera (see Fig. 1) based on which the robot has to learn to solve tasks fully autonomously. The agent perceives that a task is completed when a desired reference video frame is obtained. Therefore, this setting is an instance of the pixels-to-torques problem.

3. Deep Dynamical Model

Our approach to solve the objective defined in Section 2 is based on a deep dynamical model (DDM), which (i) embeds high-dimensional images in a low-dimensional feature space via deep auto-encoders and (ii) learns a predictive forward model in this feature space. In particular, we consider a DDM with control inputs u and high-dimensional pixel observations y . We assume that the relevant properties of y can be compactly represented by a low-dimensional feature variable z . The two components of the DDM, i.e., the prediction model, which relates the current observation y_t to past observations and control inputs (see Fig. 1) and the low-dimensional embedding of pixel information are detailed in the following.

3.1. Prediction Model

We assume the current feature value z_t to depend on past features and past control inputs. A pragmatic way to view such a model is as a way to predict the feature at time t based on past observations up to time $t - 1$ by means of

$$\hat{z}_{t|t-1}(\theta_p) = l(z_{t-1}, u_{t-1}, \dots, z_{t-n}, u_{t-n}; \theta_p), \quad (1)$$

where l is a nonlinear function, in our case a feed-forward neural network, and θ_p are the corresponding model parameters. In the system identification literature, this is known as a nonlinear autoregressive exogenous model (NARX)

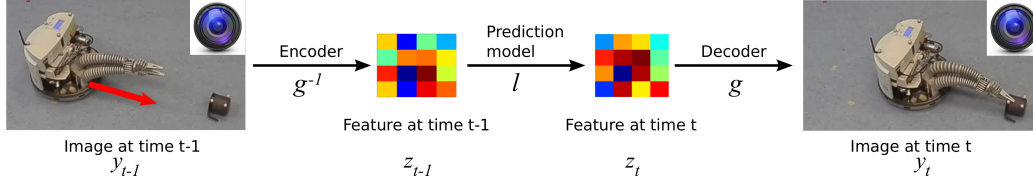


Figure 1. Illustration of our idea of combining deep learning architectures for feature learning and prediction models in feature space. A camera observes a robot approaching an object. A good low-dimensional feature representation of an image is important for learning a predictive model if the camera is the only sensor available.

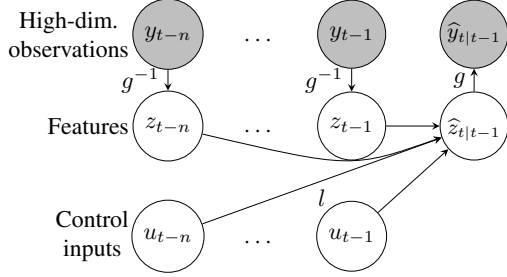


Figure 2. Prediction model: The predicted feature $\hat{z}_{t|t-1}$ is a function of the n past features z_{t-n}, \dots, z_{t-1} and control inputs u_{t-n}, \dots, u_{t-1} . Each of the features z_{t-n}, \dots, z_{t-1} is computed from high-dimensional data y_{t-n}, \dots, y_{t-1} via the encoder g^{-1} . The predicted feature $\hat{z}_{t|t-1}$ is mapped to high-dimensional prediction via the decoder g .

(Ljung, 1999). The predictive performance of the model will be important for control (see Section 6) and learning by means of a prediction-error method (Ljung, 1999).

Thus far, we can predict features from previous features and controls via (1). However, we require a model to predict observations y_t . For this purpose we define an explicit functional relationship between features and observations, a deep decoder $y = g(z; \theta_D)$. The deep decoder g maps features z to high-dimensional observations y parameterized by θ_D . Similarly, we define a deep encoder $z = g^{-1}(y; \theta_E)$ that maps high-dimensional observations y to features z parameterized by θ_E . Encoder and decoder are ideally the inverse to each other and together they form the deep auto-encoder (Hinton & Salakhutdinov, 2006). The deep auto-encoder suits our system identification problem very well, since it provides an explicit expression of both the mapping g as well as its approximate inverse g^{-1} , which we need for the predictions in (3).

Now, we are ready to put the pieces together: The feature prediction model (1) together with the deep decoder and encoder yield the prediction model for the observations

$$z_{t-1}(\theta_E) = g^{-1}(y_{t-1}; \theta_E), \quad (2)$$

$$\hat{z}_{t|t-1}(\theta_E, \theta_P) = l(z_{t-1}(\theta_E), u_{t-1}, \dots, z_{t-n}(\theta_E), u_{t-n}; \theta_P),$$

$$\hat{y}_{t|t-1}(\theta_E, \theta_D, \theta_P) = g(\hat{z}_{t|t-1}(\theta_E, \theta_P); \theta_D), \quad (3)$$

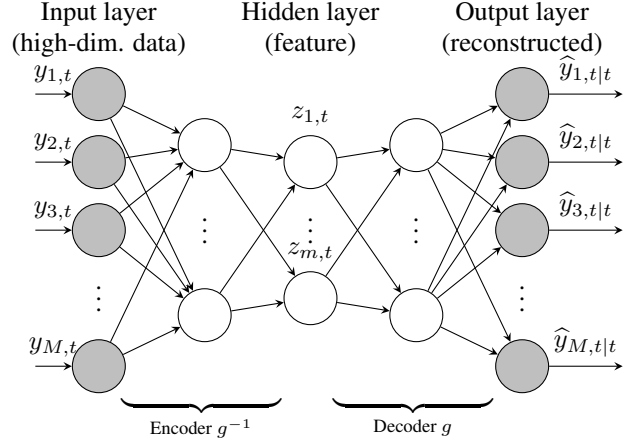


Figure 3. Auto-encoder consisting of an encoder g^{-1} and a decoder g . The original image $y_t = [y_{1,t}, \dots, y_{M,t}]^T$ is mapped onto its low-dimensional representation $z_t = [z_{1,t}, \dots, z_{m,t}]^T = g^{-1}(y_t)$ with the encoder, and then back to a high-dimensional representation $\hat{y}_{t|t-1} = g(\hat{z}_{t|t-1})$ by the decoder g , $m \ll M$.

which is also illustrated in Fig. 2. With this prediction model we define the corresponding prediction error

$$\varepsilon_t^P(\theta_E, \theta_D, \theta_P) = y_t - \hat{y}_{t|t-1}(\theta_E, \theta_D, \theta_P), \quad (4)$$

where y_t is the observed image at time t .

3.2. Deep Auto-Encoder

We employ deep auto-encoder neural networks both for the encoder g^{-1} and for the decoder g . Each layer k of the encoder neural network g^{-1} computes $y_t^{(k+1)} = \sigma(A_k y_t^{(k)} + b_k)$, where σ is an activation function¹ and A_k and b_k are free parameters. The control input to the first layer is the image, i.e., $y_t^{(1)} = y_t$. The last layer is the low-dimensional feature representation of the image $z_t(\theta_E) = g^{-1}(y_t; \theta_E)$, where $\theta_E = [\dots, A_k, b_k, \dots]$ are the parameters of all neural network layers. The decoder g consists of the same number of layers in reverse order, see Fig. 3, and can be considered an approximate inverse of the

¹We used $\sigma(x) = \arctan(x)$.

encoder g , such that $\hat{y}_{t|t}(\theta_E, \theta_D) \approx y_t$, where

$$\hat{y}_{t|t}(\theta_E, \theta_D) = g(g^{-1}(y_t; \theta_E); \theta_D) \quad (5)$$

is the reconstructed version of y_t . The encoder and the decoder are trained jointly in such a way that they minimize the sum of the squared reconstruction error

$$\varepsilon_t^R(\theta_E, \theta_D) = y_t - \hat{y}_{t|t}(\theta_E, \theta_D), \quad (6)$$

where the parameters θ_D and θ_E of g and g^{-1} optionally can be coupled to constrain the solution to some degree (Vincent et al., 2008). However, this coupling has not been used in this paper.

4. Training

Our DDM contains the following free parameters: the encoder parameters θ_E , the decoder parameters θ_D and the parameters of the prediction model θ_P . To train the model, we employ two cost functions, the sum of the squared prediction errors (4),

$$V_P(\theta_E, \theta_D, \theta_P) = \sum_{t=1}^N \|\varepsilon_t^P(\theta_E, \theta_D, \theta_P)\|^2, \quad (7a)$$

and the sum of the squared reconstruction errors (6),

$$V_R(\theta_E, \theta_D) = \sum_{t=1}^N \|\varepsilon_t^R(\theta_E, \theta_D)\|^2. \quad (7b)$$

Normally when features are used for inference of dynamical models, they are first extracted from the data in a pre-processing step by minimizing (7b) with respect to the auto-encoder parameters θ_E, θ_D . In a second step, the parameters θ_P of the prediction model are estimated based on these features by minimizing (7a) conditioned on the estimated auto-encoder parameters $\hat{\theta}_E$ and $\hat{\theta}_D$. In our experience, a potential problem with this approach is that the learned features might have a small reconstruction error, seriously complicate learning the prediction model.

Therefore, we propose to learn all model parameters $\theta_E, \theta_D, \theta_P$ jointly. For this purpose, we define the optimization problem

$$(\hat{\theta}_E, \hat{\theta}_D, \hat{\theta}_P) = \arg \min_{\theta_E, \theta_D, \theta_P} (V_R(\theta_E, \theta_D) + V_P(\theta_E, \theta_D, \theta_P)), \quad (8)$$

where we jointly optimize the free parameters in both the deep auto-encoder θ_E, θ_D and the prediction model θ_P . The required gradients with respect to all parameters can be computed efficiently by back-propagation. The cost functions are then minimized by the BFGS algorithm (Nocedal & Wright, 2006). Note that it is crucial to include not only the prediction error in (8), but also the reconstruction error. Without this term the multi-step ahead prediction performance will decrease since predicted features are not consistent with features achieved from the encoder. Since we consider a control problem in this paper, multi-step ahead predictive performance is of the essence.

Initialization. The auto-encoder has strong similarities with principal component analysis (PCA): With a linear activation function the auto-encoder and the PCA are identical (Bourlard & Kamp, 1988). We exploit this relationship to initialize the parameters of the auto-encoder: The auto-encoder network has been unfolded, each pair of layers in the encoder and the decoder have been combined, and the corresponding PCA solution has been computed for each of these pairs. We start with high-dimensional image data at the top layer and use the principal components from that pair of layers as input to the next pair of layers. Thereby, we recursively compute a good initialization for all parameters in the auto-encoder network. Similar pre-training routines are found in Hinton & Salakhutdinov (2006) where a restricted Boltzmann machine is used instead of PCA.

In the last two sections, we have presented a DDM, which facilitates fast predictions of high-dimensional observations via a low-dimensional embedded time series. System identification results based on this model are presented in Section 7.1. The property of fast predictions will be exploited by the feedback strategy presented in the following.

5. Model Predictive Control

Model predictive control (MPC) has been an active area within the automatic control community since the 1970s and first emerged in process industries (Qin & Badgwell, 2003). With increasing computational resources, MPC is today emerging in many applications with much faster dynamics, such as for example control of unmanned aerial vehicles. One important reason for its popularity is the relative ease with which constraints can be incorporated. Even though the formulation is fairly simple, many successful examples has shown that it can learn fairly complex control strategies, which makes it suitable for autonomous learning. Mayne (2014) gives an excellent overview on the present state of MPC. The textbooks by Maciejowski (2002) and Rawlings & Mayne (2009) also provide good introductions to MPC.

More specifically, in applying MPC to deterministic, non-linear, discrete-time systems, a state-space model of the system is considered

$$x_{t+1} = f(x_t, u_t), \quad y_t = h(x_t), \quad (9)$$

where the state x_t at time instance t is assumed to be known. At each time instance t , a finite-horizon optimal control problem is solved over future control inputs

$$\mathbf{u}_t^0 = \arg \min_{\mathbf{u}_t} V_N(\mathbf{u}_t), \quad (10a)$$

$$V_N(\mathbf{u}_t) = \sum_{p=0}^{P-1} f_0(\hat{x}_{t+p|t}, u_{t+p}), \quad (10b)$$

where $f_0(\hat{x}_{t+p|t}, u_{t+p})$ is a cost term associated with control. This term can for example be used to penalize deviation

from a desired reference signal.² After solving this optimization problem at each time instance t , the first control input is used in the feedback loop $u_t = u_t^0(x_t)$.

At the core of the MPC formulation lies the dynamical model of the system, which is used to predict future observations from suggested control inputs $\mathbf{u}_t = [u_t, \dots, u_{t+N-1}]$. Thus, the performance of the controller is bound to the prediction quality of the dynamical model. Adaptive control allows us to update the model as new data arrives. [Mayne \(2014\)](#) states that this type of adaptive MPC has received very little attention in the literature, and much remains to be done. [Sha \(2008\)](#) advocate a neural network approach similar to ours. A similar prediction model as in (1) has been implemented, and the parameters of the neural network are updated online along with the future control inputs using MPC in an adaptive fashion. However, they do not consider high-dimensional data and assume that they have direct access to low-dimensional measurements.

We will now turn over to describe how (adaptive) MPC can be used together with our DDM to address the pixels-to-torques problem.

6. Adaptive MPC in Feature Space

To apply adaptive MPC in our scenario where we observe high-dimensional images, we exploit the DDM introduced in Section 3 to turn MPC on images into MPC on features. In particular, we predict future features based on the optimal controls determined at each time step by MPC. By comparing (9) with (1), we define the state as the present and past features together with past control inputs, i.e.,

$$x_t = [z_t, z_{t-1}, \dots, z_{t-n+1}, u_{t-1}, \dots, u_{t-n}].$$

The features are computed with the encoder $z_{t-i} = g^{-1}(y_{t-i}, \theta_E)$. Therefore, we can assume that x_t is known at time instance t , as done in deterministic MPC. Shifting the MPC problem to feature space has the appealing side effect that predictions can be performed efficiently.

Our objective is to control the system towards a desired reference image frame y_{ref} . Also the reference frame y_{ref} can be encoded to a reference feature $z_{\text{ref}} = g^{-1}(y_{\text{ref}}, \theta_E)$ by using the encoder.

6.1. Control

We implemented a nonlinear MPC solution by using

$$f_0(\hat{x}_{t+p|t}, u_{t+p}) = \|\hat{z}_{t+p|t} - z_{\text{ref}}\|^2 + \lambda \|u\|^2 \quad (11)$$

²In the more generic description of MPC we can also easily include constraints on the state and control signal in (10a). It is also common to include an addition penalty term penalizing the final state $\hat{x}_{t+N|t}$ in order to achieve stability ([Mayne et al., 2000](#)). However, non of these terms will be used in this work.

as presented in Section 5. The first term in (11) ensures good tracking performance, whereas the second term is a control penalty, which plays the role of a regularizer. The gradients of the cost function (10a) with respect to future control inputs can be computed efficiently by back-propagation, such that BFGS can be used to find the optimal sequence of control signals. However, care has to be taken since $V_N(\mathbf{u}_t)$ depends on \mathbf{u}_t not only via the term u_{t+i} in $f_0(\hat{z}_{t+p|t}, u_{t+p})$, but also via the predictions $\hat{z}_{t+p|t}$ by recursively using the prediction part (3) of the DDM.

6.2. Exploration-Exploitation Trade-Off

We want to use the MPC controller in an adaptive fashion to gradually improve the model by collected data in the feedback loop without any specific prior knowledge of the system at hand. However, the standard application of adaptive control and adaptive MPC is not to learn models from scratch, but rather to adapt to slowly varying changes in model parameters. Simply applying the MPC controller based on a randomly initialized model would make the closed loop system very likely to converge to a point which is far away from the desired reference value, due to the poor model. This would in turn result in that nearly no data is collected from the region that we actually are interested in. In our setting, we therefore need a trade-off between exploration and exploitation to ensure the excitation of the system. We chose an ϵ -greedy exploration strategy where the optimal feedback u_t^0 is chosen with a probability $1 - \epsilon$, and a random action is chosen with probability ϵ .

6.3. Iterative Model Learning

The data collection is performed in closed-loop and is divided into multiple sequential trials. After each trial, we add the data of the most recent trajectory to the data set and the model is re-trained using all data that has been collected so far. To account for previously collected data, we adapt the optimization problem (8) to

$$(\hat{\theta}_E, \hat{\theta}_D, \hat{\theta}_M) = \arg \min_{\theta_E, \theta_D, \theta_P} (\bar{V}_R(\theta_E, \theta_D) + \bar{V}_P(\theta_E, \theta_D, \theta_P)), \quad (12)$$

where the prediction error term \bar{V}_P is the average of all prediction error terms from all trials, i.e.,

$$\bar{V}_P(\theta_E, \theta_D, \theta_P) = \sum_{i=1}^I \frac{N_i}{\sum_{i=1}^I N_i} V_P(\theta_E, \theta_D, \theta_P; Y_i), \quad (13)$$

where Y_i are the measurements collected in the i th trial. The reconstruction error term

$$\bar{V}_R(\theta_E, \theta_D) = \bar{V}_R(\theta_E, \theta_D; Y_1, \dots, Y_I) \quad (14)$$

uses all data collected so far. The final procedure is summarized in Algorithm 1.

Algorithm 1 Adaptive MPC in feature space

Follow a random control strategy and record data
for $i = 1$ to L **do**
 Update DDM with all data collected so far using (12).
for $t = 0$ to $N - 1$ **do**
 $u_t^* \leftarrow \epsilon$ -greedy MPC policy based on DDM prediction
 Apply u_t^* and record data
end for
end for

7. Experimental Results

In the following, we empirically assess the components of our proposed methodology for autonomous learning on high-dimensional synthetic image data. First, we show that good DDMs (see Section 3) can be learned from pixel information only. Second, following the ideas from Section 6, we demonstrate the viability of our approach to learn from pixels to torques: The learner automatically finds good continuous controls (torques) for a simulated pendulum where screenshots (pixels) are the only measurements available. We compare our approach with PILCO (Deisenroth & Rasmussen, 2011), a state-of-the-art RL method for data efficient closed-loop policy learning in continuous state and action spaces.

In both examples, we learn the DDM solely based on images with $51 \times 51 = 2601$ pixels in each frame. Each pixel $y_t^{(i)}$ is a component of the measurement $y_t = [y_t^{(1)}, \dots, y_t^{(2601)}]^\top$ and assumes a continuous gray-value within the interval $[0, 1]$.

7.1. Long-Term Predictions with the DDM

To assess the predictive performance of the DDM, we simulated 601 frames of a moving tile on the screen, see Fig. 4. The control inputs are the (random) increments in position in horizontal and vertical directions. The image sequence was reduced to $\dim(y_t) = 50$ prior to the parameter learning using PCA. A four-layer 50-25-12-8-2 auto-encoder (5) was used to learn two-dimensional features, and an 8-5-2 feed-forward neural network for the prediction model in the latent space (1) using $n = 2$.

We evaluate the performance of the learned DDM in terms of long-term predictions, which will play a central role in MPC for autonomous learning. Long-term predictions are obtained by concatenating multiple 1-step ahead predictions. The performance of DDM is illustrated in Fig. 4 on a test data set. The top row shows the ground truth images and the bottom row shows the DDM’s long-term predictions. The model predicts future frames of the tile with high accuracy both for 1-step ahead and multiple steps ahead.

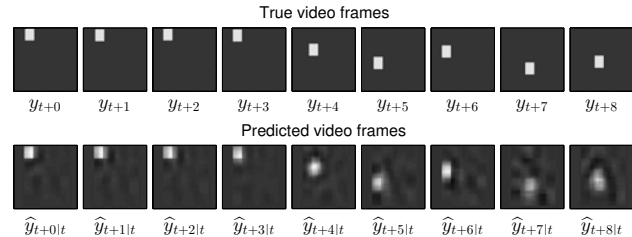


Figure 4. Long-term (up to eight steps) predictive performance of the DDM: True (upper plot) and predicted (lower plot) video frames on test data.

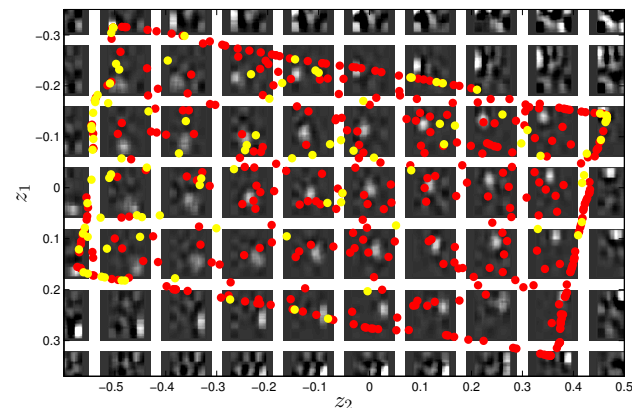


Figure 5. Identification: Feature space zoomed in to the region $z \in [-0.35, 0.35] \times [-0.5, 0.5]$, divided into 10×7 grid points. For each grid point the decoded high-dimensional image is displayed. The training (red) and validation (yellow) data reside on a two-dimensional manifold corresponding to the two-dimensional position of the tile.

In Fig. 5, the feature representation of the data is displayed. The features reside on a two-dimensional manifold encoding the two-dimensional position of the moving tile. This structure is induced by the joint training of the auto-encoder and the prediction model. The corresponding feature representation for the case of separate learning does not exhibit such a structure, Appendix A.

7.2. Learning Torques from Pixels: Planar Pendulum

In this section, we report results on learning optimal torques u for a planar pendulum (1-link robot arm with length 1 m, weight 1 kg and friction coefficient 1 Nsm/rad), purely based on pixel information. For this purpose, we simulated the pendulum and took screenshots of its behavior. The learning algorithm only had access to pixel values from of these screenshots, based on which it had to learn a policy that moves the pendulum from a start position $\varphi = 0$ to a target position $\varphi = \pm\pi$. The reference signal was the screenshot corresponding to the target position. We used a sampling frequency of $T = 0.2$ s and a time horizon of

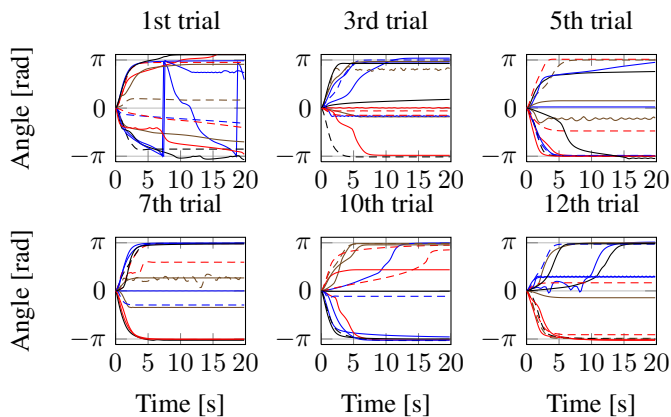


Figure 6. Control performance after 1st to 12th trial evaluated with $\epsilon = 0$ of all 14 different experiments. The objective was to reach an angle of $\pm\pi$.

25 s, which corresponds to 100 frames per trial.

The input dimension has been reduced to $\dim(y_t) = 50$ prior to model learning using PCA. With these 50-dimensional inputs, a four-layer auto-encoder network was used with dimension 50-25-12-6-2, such that the features were of dimension $\dim(z_t) = 2$. The order of the dynamics was chosen to $n = 2$ to capture velocity information, such that $z_t = l(z_{t-1}, u_{t-1}, z_{t-2}, u_{t-2})$. For the prediction model l we used a two-layer neural network with a 6-4-2 architecture. For the MPC controller, we used a planning horizon of $P = 15$ steps and a control penalty $\lambda = 0.01$. For the ϵ -greedy exploration strategy we used $\epsilon = 0.2$. We conducted 14 independent experiments with different random initializations. The learning algorithm was run for 13 trials (learning episodes). After each trial, we retrained the DDM using all collected data so far.

To assess the controller performance after each trial, we applied a greedy policy ($\epsilon = 0$). In Fig. 6, angle trajectories of all experiments at different learning stages are displayed. Already in the first trial, the controller managed in 5 out of the 14 experiments to drive the pendulum toward the reference value $\pm\pi$. The control performance increased gradually with the number of trials and after the 12th trial, 10 out of the 14 experiments manage to solve the task.

To quantify this improvement, we define the steady-state error as the absolute difference between the reference angle and the final angle. In Fig. 7 (top) the average steady-state error over all experiments is shown. This graph indicates a decreasing trend in the steady-state error as learning progresses. We also define the rise time as the time it takes for the angle to go from 10% to 90% of the desired angle. Fig. 7 (bottom) shows the rise time. Both average steady-state error and rise time show a decreasing error and

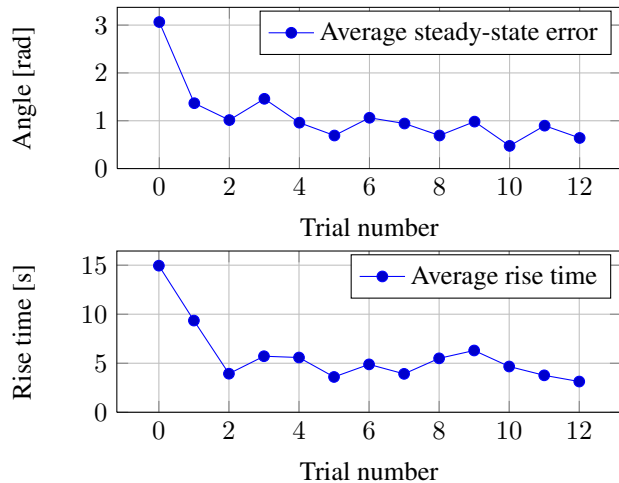


Figure 7. Steady-state error (top) and rise time (bottom) averaged using over 14 experiments.

increasing speed, which indicates that the controller and model quality improve with the data/experience collected.

Fig. 8 displays the “decoded” images corresponding to the latent representations after all 13 trials. The feature values of the training data (green) line up in a circular shape enabling a low-dimensional dynamical description. The DDM extracts features that can also model the *dynamic* behavior compactly. Also the prediction produced by the MPC controller is displayed. By making use of the DDM, the controller can determine an optimal feedback for controlling the pendulum towards the reference value.

7.3. Comparison with PILCO RL Framework

As a comparison, we applied the PILCO RL framework (Deisenroth & Rasmussen, 2011) to learning closed-loop control policies for the pendulum task above. We used the same simulation parameters as before.

PILCO is the current state-of-the-art RL algorithm for data-efficient learning control policies in continuous state-control spaces. Using collected data PILCO learns a probabilistic model for the system dynamics, implemented as a Gaussian process (Rasmussen & Williams, 2006). Subsequently, this model is used to compute a distribution over trajectories and the corresponding expected cost for a given policy parameterization. With this, the controller parameters are optimized. PILCO’s explicit incorporation of model uncertainty into planning and decision making enables it to learn complex nonlinear policies for robotic systems in only a few trials (Deisenroth et al., 2014). Although PILCO uses data very efficiently, its computational demand makes its direct application impractical for high-dimensional ($\gg 20$ D) problems, including the pixels-to-

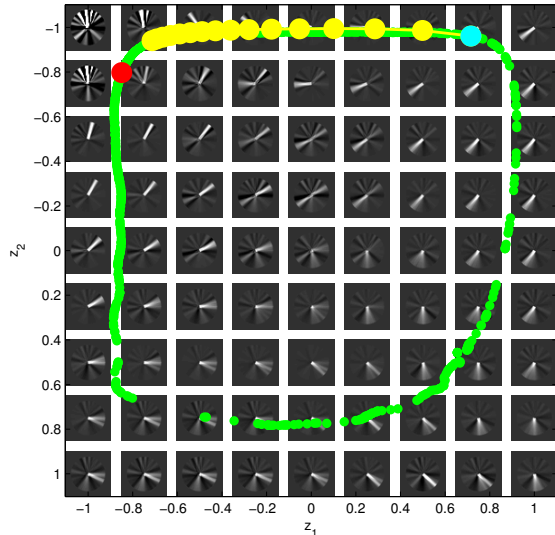


Figure 8. The feature space $z \in [-1, 1] \times [-1, 1]$ is divided into 9×9 grid points for illustration purposes. For each grid point the decoded high-dimensional image is displayed. Different 2D feature values are overlaid. Green: Feature values corresponding to collected experience in previous trials. Cyan: Feature value corresponding at current time step during a control sequence. Red: Desired reference value. Yellow: 15 steps ahead prediction after optimizing for the optimal control inputs.

torques problem considered in this paper.³

To apply PILCO in the considered setting of learning torques from pixel information, we used a deep auto-encoder (same setting as above) to learn a compact (2D) representation z of the image y . Subsequently, we trained a GP model for the forward/transition dynamics in this feature space, such that $x_{t+1} = f(x_t, u_t)$ where we defined the state $x_t = [z_t, z_{t-1}]$ to account for velocities, which are not captured by a static image. Typical trajectories from this experiment are shown in Fig. 7.3. Clearly, this approach is not successful, and there is very little hope that its performance will improve with number of trials.

Fig. 10 displays the average success rate of PILCO (including standard error) and our proposed method using deep dynamical models together with a tailored MPC (DDM+MPC). As a ground-truth baseline, we include PILCO trained on the “true” state $(\varphi, \dot{\varphi})$ in a standard RL setting (blue). We define “success” if the steady-state error of the pendulum’s angle is below 10%. The graph shows that our proposed algorithm (brown) is not too far

³We did apply PILCO to learning policies for the pendulum task directly on pixel information, where we applied a random projection matrix to lower the dimension of each image to 20 dimensions. After 12 trials and a few days of training, PILCO did not show any learning progress.

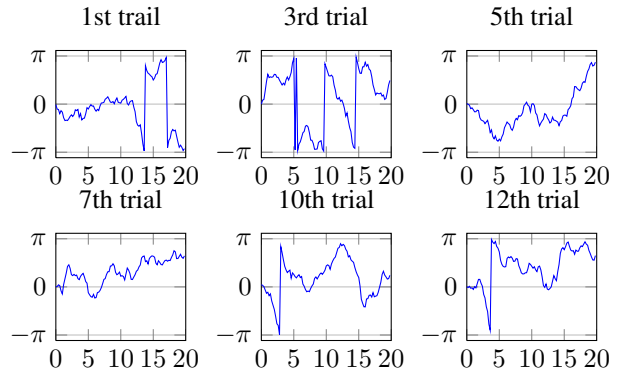


Figure 9. PILCO’s performance with auto-encoder (AE) features. Since the AE features do not capture the dynamic behavior, PILCO cannot learn a good policy at all.

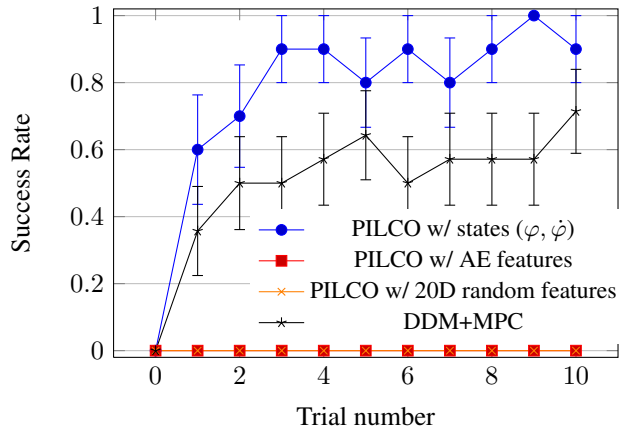


Figure 10. Blue: PILCO ground-truth baseline using the true state $(\varphi, \dot{\varphi})$. Red: PILCO using learned auto-encoder features from image pixels. Brown: PILCO on 20D features computed with PCA. Black: Our proposed MPC solution using the DDM.

behind the ground-truth solution. However, PILCO trained on the auto-encoder features (red) fails consistently in all experiments. We explain PILCO’s failure by the fact that we trained the auto-encoder and the transition dynamics in feature space separately. The auto-encoder finds (really) good features that minimize the reconstruction error. However, these features are not good for modeling the dynamic behavior of the system,⁴ and lead to a bad long-term predictions. Even a GP cannot cope with this problem.

8. Conclusion

We have proposed a data-efficient model-based RL algorithm that learns closed-loop policies in continuous state

⁴When we inspected the latent-space embedding of the auto-encoder, the pendulum angles do not nicely line up along an “easy” manifold as in Fig. 8.

and action spaces directly from pixel information. The key components of our solution are (1) a deep dynamical model (DDM) that is used for long-term predictions in a compact feature space and (2) an MPC controller that uses the predictions of the DDM to determine optimal actions. For the success of this RL algorithm it is crucial that the DDM learns the feature mapping and the predictive model in feature space jointly to capture dynamic behavior for high-quality long-term predictions. Compared to state-of-the-art RL our algorithm learns quickly, scales to high-dimensional state spaces and facilitates learning from pixels to torques.

Acknowledgments

This work was supported by the Swedish Foundation for Strategic Research under the project Cooperative Localization and the Swedish Research Council under the project Probabilistic modeling of dynamical systems (Contract number: 621-2013-5524). MPD was supported by an Imperial College Junior Research Fellowship.

References

- Atkeson, Christopher G. and Schaal, S. Learning Tasks from a Single Demonstration. In *Proceedings of the IEEE International Conference on Robotics and Automation*, volume 2, pp. 1706–1712, 1997.
- Bagnell, James A. and Schneider, Jeff G. Autonomous Helicopter Control using Reinforcement Learning Policy Search Methods. In *Proceedings of the International Conference on Robotics and Automation*, pp. 1615–1620. IEEE, 2001.
- Bengio, Yoshua, Lamblin, Pascal, Popovici, Dan, and Larochelle, Hugo. Greedy Layer-Wise Training of Deep Networks. In *NIPS*, 2007.
- Bourlard, Hervé and Kamp, Yves. Auto-association by multilayer perceptrons and singular value decomposition. *Biological cybernetics*, 59(4-5):291–294, 1988.
- Brock, Oliver. *Berlin Summit on Robotics: Conference Report*, chapter Is Robotics in Need of a Paradigm Shift?, pp. 1–10. December 2011.
- Deisenroth, Marc P. and Rasmussen, Carl E. PILCO: A Model-Based and Data-Efficient Approach to Policy Search. In *Proceedings of the International Conference on Machine Learning*, pp. 465–472. ACM, June 2011.
- Deisenroth, Marc P., Fox, Dieter, and Rasmussen, Carl E. Gaussian Processes for Data-Efficient Learning in Robotics and Control. *IEEE Transactions on Pattern Analysis and Machine Intelligence*, 36, 2014. doi: 10.1109/TPAMI.2013.218.
- Hinton, G and Salakhutdinov, R. Reducing the dimensionality of data with neural networks. *Science*, 313:504–507, 2006.
- Lange, Sascha and Riedmiller, Martin. Deep Auto-Encoder Neural Networks in Reinforcement Learning. In *Proceedings of the International Joint Conference on Neural Networks*, 2010.
- LeCun, Y, Bottou, L, Bengio, Y, and Haffner, P. Gradient-based learning applied to document recognition. *Proceedings of the IEEE*, 86(11):2278–2324, 1998.
- Ljung, L. *System identification, Theory for the user*. System sciences series. Prentice Hall, Upper Saddle River, NJ, USA, second edition, 1999.
- Maciejowski, J. M. *Predictive Control with Constraints*. Prentice Hall, 2002.
- Mayne, David Q. Model predictive control: Recent developments and future promise. *Automatica*, 50(12):2967–2986, 2014.
- Mayne, David Q, Rawlings, James B, Rao, Christopher V, and Scokaert, Pierre OM. Constrained model predictive control: Stability and optimality. *Automatica*, 36(6):789–814, 2000.
- Mnih, Volodymyr, Kavukcuoglu, Koray, Silver, David, Graves, Alex, Antonoglou, Ioannis, Wierstra, Daan, and Riedmiller, Martin. Playing Atari with Deep Reinforcement Learning. arXiv:1312.5602, December 2013.
- Nocedal, J. and Wright, S. J. *Numerical Optimization*. Springer Series in Operations Research. New York, USA, 2 edition, 2006.
- Pan, Yunpeng and Theodorou, Evangelos. Probabilistic Differential Dynamic Programming. In *Advances in Neural Information Processing Systems*, 2014.
- Qin, S Joe and Badgwell, Thomas A. A survey of industrial model predictive control technology. *Control engineering practice*, 11(7):733–764, 2003.
- Rasmussen, Carl E. and Williams, Christopher K. I. *Gaussian Processes for Machine Learning*. Adaptive Computation and Machine Learning. The MIT Press, Cambridge, MA, USA, 2006.
- Rawlings, J. B. and Mayne, D. Q. *Model predictive control: theory and design*. Nob Hill Publishing, 2009.
- Sha, Daohang. A new neural networks based adaptive model predictive control for unknown multiple variable non-linear systems. *International Journal of Advanced Mechatronic Systems*, 1(2):146–155, 2008.

Sutton, Richard S. and Barto, Andrew G. *Reinforcement Learning: An Introduction*. Adaptive Computation and Machine Learning. The MIT Press, Cambridge, MA, USA, 1998.

Vincent, P, Larochelle, H, Bengio, Y, and Manzagol, Pierre-Antoine. Extracting and composing robust features with denoising autoencoders. In *Proceedings of the 25th International Conference on Machine Learning (ICML)*, Helsinki, Finland, 2008.

A. Results of Separately Learning Features and Dynamics

In the first experiment in the paper, results of joint learning of prediction and reconstruction error have been reported. Joint learning brings structure to feature values, which is not present if the auto-encoder is learned separately, see Fig. 11.

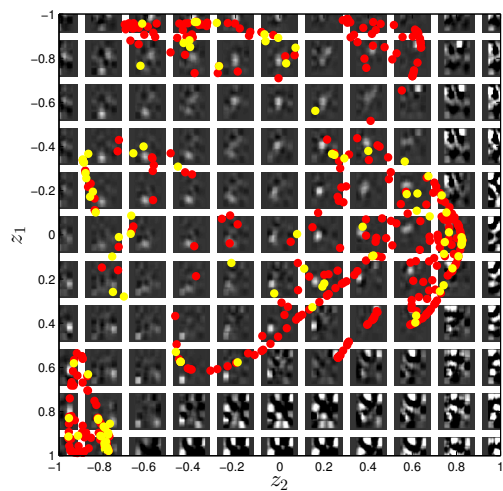


Figure 11. The feature space in the region $z \in [-1, 1] \times [-1, 1]$ for separate learning. The training (red) and validation (yellow) data do not reside on a structured two-dimensional tile-formed manifold as it was the case for the joint learning in Fig. 5.